

Mixed mode oscillations in presence of inverted fireball in an excitable DC glow discharge magnetized plasma

Vramori Mitra, N. Hari Prakash, Infant Solomon, Mariammal Megalingam, A. N. Sekar Iyengar, Norbert Marwan, Jürgen Kurths, Arun Sarma, and Bornali Sarma

Citation: [Physics of Plasmas](#) **24**, 022307 (2017); doi: 10.1063/1.4976320

View online: <http://dx.doi.org/10.1063/1.4976320>

View Table of Contents: <http://aip.scitation.org/toc/php/24/2>

Published by the [American Institute of Physics](#)

Articles you may be interested in

[Continuum kinetic and multi-fluid simulations of classical sheaths](#)
[Physics of Plasmas](#) **24**, 022118022118 (2017); 10.1063/1.4976544

[Spontaneous emission of electromagnetic fluctuations in magnetized plasmas](#)
[Physics of Plasmas](#) **24**, 022117022117 (2017); 10.1063/1.4976321

[Ion temperature effects on its chaotic behavior in ion-sheath](#)
[Physics of Plasmas](#) **24**, 022301022301 (2017); 10.1063/1.4975316

[Floating potential measurements in plasmas: From dust to spacecraft](#)
[Physics of Plasmas](#) **24**, 023701023701 (2017); 10.1063/1.4975610



VACUUM SOLUTIONS FROM A SINGLE SOURCE

Pfeiffer Vacuum stands for innovative and custom vacuum solutions worldwide, technological perfection, competent advice and reliable service.

Mixed mode oscillations in presence of inverted fireball in an excitable DC glow discharge magnetized plasma

Vramori Mitra,¹ N. Hari Prakash,¹ Infant Solomon,¹ Mariammal Megalingam,¹ A. N. Sekar Iyengar,² Norbert Marwan,³ Jürgen Kurths,^{3,4} Arun Sarma,¹ and Bornali Sarma¹

¹VIT University, Vandalur- Kelambakkam Road, Chennai 600 127, Tamilnadu, India

²Saha Institute of Nuclear Physics, 1/AF Bidhannagar, Calcutta 700 064, India

³Potsdam Institute for Climate Impact Research, D-14415 Potsdam, Germany

⁴Institute for Complex Systems and Mathematical Biology, University of Aberdeen, Aberdeen AB24 3FX, United Kingdom

(Received 27 July 2016; accepted 6 January 2017; published online 21 February 2017)

The typical phenomena of mixed mode oscillations and their associated nonlinear behaviors have been investigated in collisionless magnetized plasma oscillations in a DC glow discharge plasma system. Plasma is produced between a cylindrical mesh grid and a constricted anode. A spherical mesh grid of 80% optical transparency is kept inside a cylindrical grid to produce an inverted fireball. Three Langmuir probes are kept in the ambient plasma to measure the floating potential fluctuations at different positions of the chamber. It has been observed that under certain conditions of discharge voltages and magnetic fields, the mixed mode oscillation phenomena (MMOs) appears, and it shows a sequential alteration with the variation of the magnetic fields and probe positions. Low frequency instability has been observed consistently in various experimental conditions. The mechanisms of the low frequency instabilities along with the origin of the MMOs have been qualitatively explained. Extensive linear and nonlinear analysis using techniques such as fast Fourier transform, recurrence quantification analysis, and the well-known statistical computing, skewness, and kurtosis are carried out to explore the complex dynamics of the MMO appearing in the plasma oscillations under various discharge conditions and external magnetic fields.

Published by AIP Publishing. [<http://dx.doi.org/10.1063/1.4976320>]

I. INTRODUCTION

The plasma sheath has been studied extensively for its various applications in plasma processing, plasma turbulence, astrophysics, etc., by using analytical models, numerical simulation, and different experiments. The formation of sheath is a ubiquitous process in laboratory plasma experiments due to the inevitable contact with another material. The physics of plasma sheath instability has so far been extensively investigated.^{1–5} Experimental investigations have been performed to study the behavior of sheath instability due to a mesh grid in a double plasma device. Bornali *et al.*⁶ carried out experiments on the sheath and magnetic pre sheath in the presence of a magnetic field and reported an enhancement of the sheath thickness with the increase in the magnetic field strength. The investigations on electron-rich⁷ and ion-rich sheath oscillations^{8,9} show that the oscillations are in the electron plasma frequency and in the ion plasma frequency range, respectively. Another related phenomenon that is very much studied in the context of sheath is fireball (FB)^{10–14} and inverted fireball.^{15–17} Fireball (FB) is a glowing sheath region around a positively biased electrode. Recently, Mitra *et al.* reported the onset of normal and inverse homoclinic bifurcation in the presence of a fireball in a double plasma device.¹⁸ Inverted fireballs are considered as a luminous sheath region that forms within a highly transparent positively biased hollow grid electrode. When electrons from ambient plasma are accelerated into the spherical mesh grid, they start to ionize neutrals inside the spherical grid and form the inverted FB, i.e., the fireball is trapped inside the spherical grid.

The complex oscillations, which shift between slow and fast motion and small and large amplitudes, are considered as mixed mode oscillations (MMOs). Complex patterns, where different amplitudes of oscillations are interspersed, are ubiquitous in nature and are classified in terms of the observed patterns. The pattern characterized by large (L) and small amplitude (s) oscillations is denoted by L^s. The small and large oscillations are often elucidated as the result of the sub threshold oscillations and relaxation mechanisms of the system. There have been several examples of the appearance of MMOs in chemical systems,^{19,20} plasma systems,^{21,22} and electronics.²³ In medical sciences, MMOs are the subject of intense research as it is often observed in different neuronal activities. Recently, Ghosh *et al.*²⁴ reported irregular-regular-irregular MMOs in a glow discharge plasma system, and the MMOs are observed to be compound, low dimensional, and anti persistent in nature. Shaw *et al.*²⁵ investigated canard and irregular-regular mixed mode oscillations in a glow discharge plasma in the presence of an inhomogeneous magnetic field. Although MMOs have been studied in an excitable glow discharge plasma system in the presence of inhomogeneous magnetic fields, no clear evidence of continuous sequential changes of MMOs in the presence of inverted fireball and homogenous magnetic field has been reported yet.

In this work, we report the existence of continuous sequence of MMOs in the presence of anode glow (fireball) controlled by a homogeneous magnetic field in a DC glow discharge plasma system. In our experiment, the spherical cage is positively biased and the cylindrical grid is negatively

biased. A spherical glowing region (anode glow) is developed inside the spherical mesh grid, which we consider as an inverted fireball. We observed sequential changes of MMOs in the oscillations of floating potential fluctuations in three particular plasma regimes with the variation of the magnetic field and the discharge voltage. The experimental observations of the spatio temporal dynamics of the MMOs, which emerged in the floating potential fluctuations, are presented. The evolution of the MMOs is investigated extensively using various nonlinear tools, *viz.*, spectral analysis, recurrence quantification analysis (RQA), skewness, kurtosis, etc. Farey arithmetic and devil's staircase are implemented to characterize the MMO features.

The paper is organized as follows: Section II describes the experimental setup used for the experiment. In Section III, the experimental results are discussed, which illustrates the characterization of different MMOs in the plasma dynamics for different magnetic fields at two constant voltages and presents the nonlinear and statistical analysis of plasma oscillations. In Section IV, the sequences of MMOs are demonstrated by Farey arithmetic and devil's staircase. Section V concludes with a brief summary of experimental results and new possibilities of investigation.

II. EXPERIMENTAL SETUP

The experimental investigation is performed in the collisionless Argon plasma, produced in a stainless steel cylindrical chamber of 50 cm in length and 40 cm in diameter. The schematic diagram of the experimental setup is displayed in Fig. 1(a). Two mesh grids, cylindrical and spherical size of 80% optical transparency, are introduced vertically in the middle of the chamber. The cylindrical mesh grid is kept negative, and the whole chamber is grounded. The spherical mesh grid acts as an anode, which is connected with the constricted electrode. An anode glow (fireball) is observed inside the spherical grid at different discharge voltages. As the spherical grid is positively biased, the electrons are accelerated towards the fireball and ionize the local plasma near the potential of the grid, while the ions are ejected away from the plasma.

The chamber is evacuated by a rotary pump to attain the base pressure of 9.2×10^{-3} mbar. Argon gas is injected by a needle valve into the chamber to acquire the working pressure of 2.3×10^{-1} mbar. The magnetic field is produced by a

Helmholtz coil, and wound around the cylindrical chamber. The current passing through the Helmholtz coil is increased up to 500 Ampere (A). A uniform axial magnetic field up to 224 G is applied to confine the ions and electrons in the plasma system. The current and magnetic field show a linear relationship as illustrated in Fig. 1(b). Finally, a discharge is struck at 240 V DC discharge voltage. The dynamical scenario of plasma oscillations of floating potential fluctuations are obtained simultaneously by three Langmuir probes (LP_1 , LP_2 , and LP_3) of diameter 0.5 mm and length 2 mm inserted in three different positions of the chamber, *viz.*, inside the spherical grid (regime I), between spherical and cylindrical grids (regime II), and outside the cylindrical grid (regime III). The signals picked up by the Langmuir probes are acquired directly in a 4 channel digital oscilloscope with a bandwidth up to 400 MHz and storage up to 2.5×10^6 samples.

Typical plasma parameters, namely, plasma density and electron temperature, for various imposed conditions are found to be the order of 10^8 – 10^9 /cc and 3–4 eV.

III. RESULTS AND DISCUSSION

The dynamics of the floating potential fluctuations are observed in different discharge voltages, *viz.*, 240 V and 250 V at a constant pressure of 2.3×10^{-1} mbar. In this experiment, the magnetic fields and the discharge voltages are considered as the control parameters. At a constant discharge voltage, the magnetic field is varied from 1 G to 198 G, and various types of MMOs are observed in the dynamics of the floating potential fluctuations obtained at three fixed positions within the hollow chamber. It is noticed that the floating potential fluctuations obtained outside the spherical ball, *i.e.*, bulk plasma regime, show a clear pattern of MMOs when compared to the other to probe signals. The evaluations of the dynamics of the MMOs are mainly studied with the help of recurrence plots (RPs) and recurrence quantification²⁶ measures, and their statistical distributions are illustrated by using skewness and kurtosis.

A. Autonomous plasma dynamics inside and outside the plasma fireball

Depending on the experimental conditions, the floating potential fluctuations appear in a wave form of mixed mode oscillations. All the signals exhibit different types of pattern,

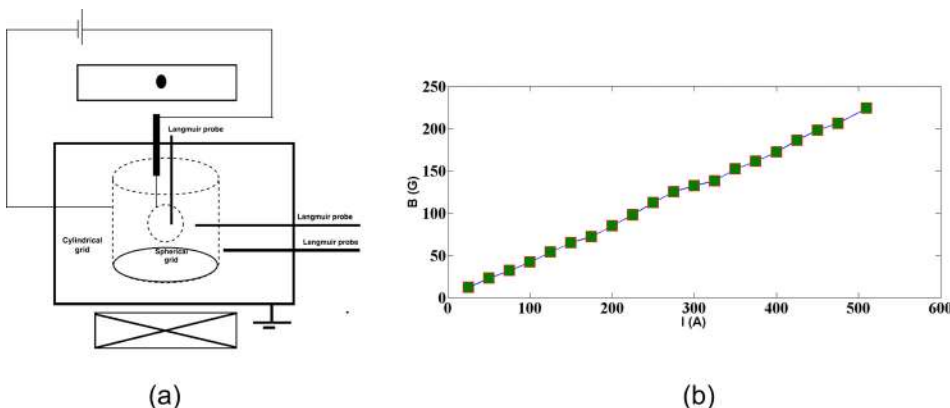


FIG. 1. (a) Schematic diagram of the experimental setup. (b) Calibration curve for the current passes through the Helmholtz coil versus the produced magnetic field.

which correspond to different types of MMOs as shown in Figs. 2 and 3.

Fig. 2(i) illustrates the emergence of the mixed mode oscillations at 240 V in the presence of a low magnetic field, in the range of 0–12 G. Figs. 2(i-a₁)–2(i-d₁) and 2(i-a₂)–2(i-d₂) represent the signals of the floating potential fluctuations obtained by the inner (LP₁) and the middle probes (LP₂), and show the transitions of the mixed mode oscillations from 1⁵ to 1³ states. Figs. 2(ii) and 2(iii) represent a detail of the 1⁵ and 1³ states and clearly reflect the number of small oscillations (5 and 3) between two consecutive large oscillations. At 240 V, changes in the mixed mode oscillations are observed in the low magnetic field regime. Moreover, we have found that from 12 G to higher magnetic fields, the mixed mode state remains constant (1³). Hence, we present only the low magnetic field regime (1 G–12 G) where different types of MMO transitions are clearly visible.

Figs. 2(i-a₃)–2(i-d₃) represent the signal of the floating potential fluctuations obtained by the outer probe (LP₃). The signal captured by the outer probe reveals that large oscillations clearly emerge, but small oscillations are irregular in nature.

Figs. 3(i-a₁)–3(i-h₁) and 3(i-a₂)–3(i-h₂) show a sequence of MMOs in regimes I and II, respectively, with the variation of the magnetic field at 250 V. The maximum amplitude of

the oscillation captured inside the sphere is around 0.4 V, while the middle probe shows values around 6 V. We are mainly focusing on the middle probe signal in regime II as the nature of the oscillation is more prominent because of more dense plasma existing in this regime. It is also evident from the amplitudes of the time series signal as displayed in Fig. 3(i). Initially, when $B = 0$, the MMO sequence emerges as 1⁸ state. When the magnetic field is further enhanced to 23 G, it corresponds to 1⁶ states; then at 70 G, the transition changes to 1⁴ states. At 76 G, the MMO sequence shows 1³ states, and this state persists up to 132 G. The MMOs transform into 1² at 164 G and then further alter to 1¹ states at 198 G and remain constant for higher magnetic fields.

The oscillations that are observed at the outer probe are more irregular and complex (Figs. 3(i-a₃)–3(i-h₃)). Small oscillations show negative spikes, while large oscillations are prominent, but the amplitude of the small oscillations is less around 0.4 V.

With the increase in the magnetic field, the number of small oscillations between two successive large oscillations gradually disappears (1⁵ to –1³ and 1⁸ to –1¹), but the large oscillations remain invariant in all of the magnetic fields (Figs. 2 and 3). It reflects that the magnetic field confines the plasma oscillations and controls its transitions to the order state. However, we find that the nature of the small

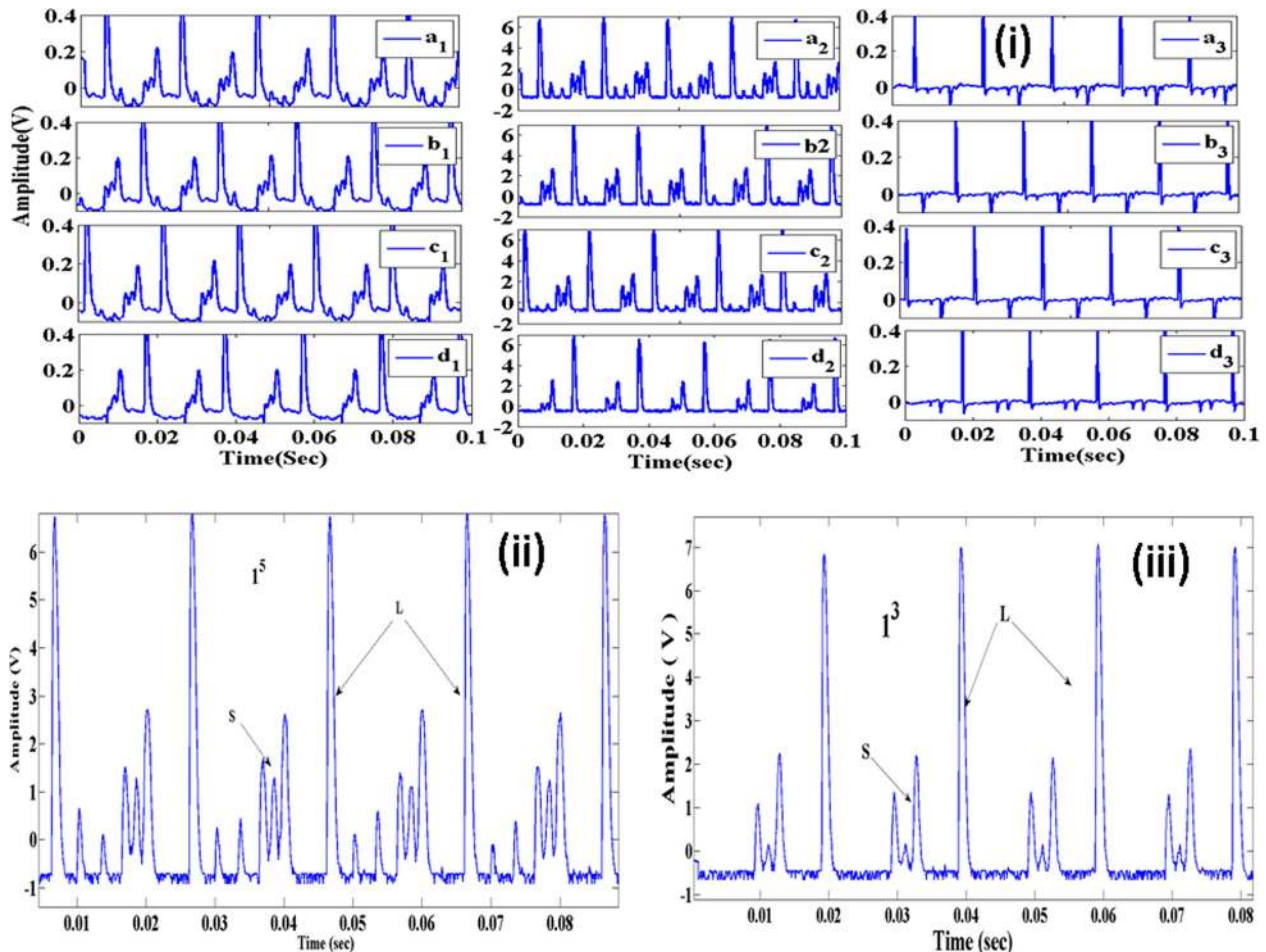


FIG. 2. (i) Signal of the floating potential fluctuations obtained by the inner (a₁)–(d₁), the middle (a₂)–(d₂), and the outer Langmuir probes (a₃)–(d₃) in various magnetic fields: (a) 0 G, (b) 4 G, (c) 8 G, and (d) 12 G at 240 V. (ii) and (iii) Shows the expanded view of the signals a₂ and d₂ of (i).

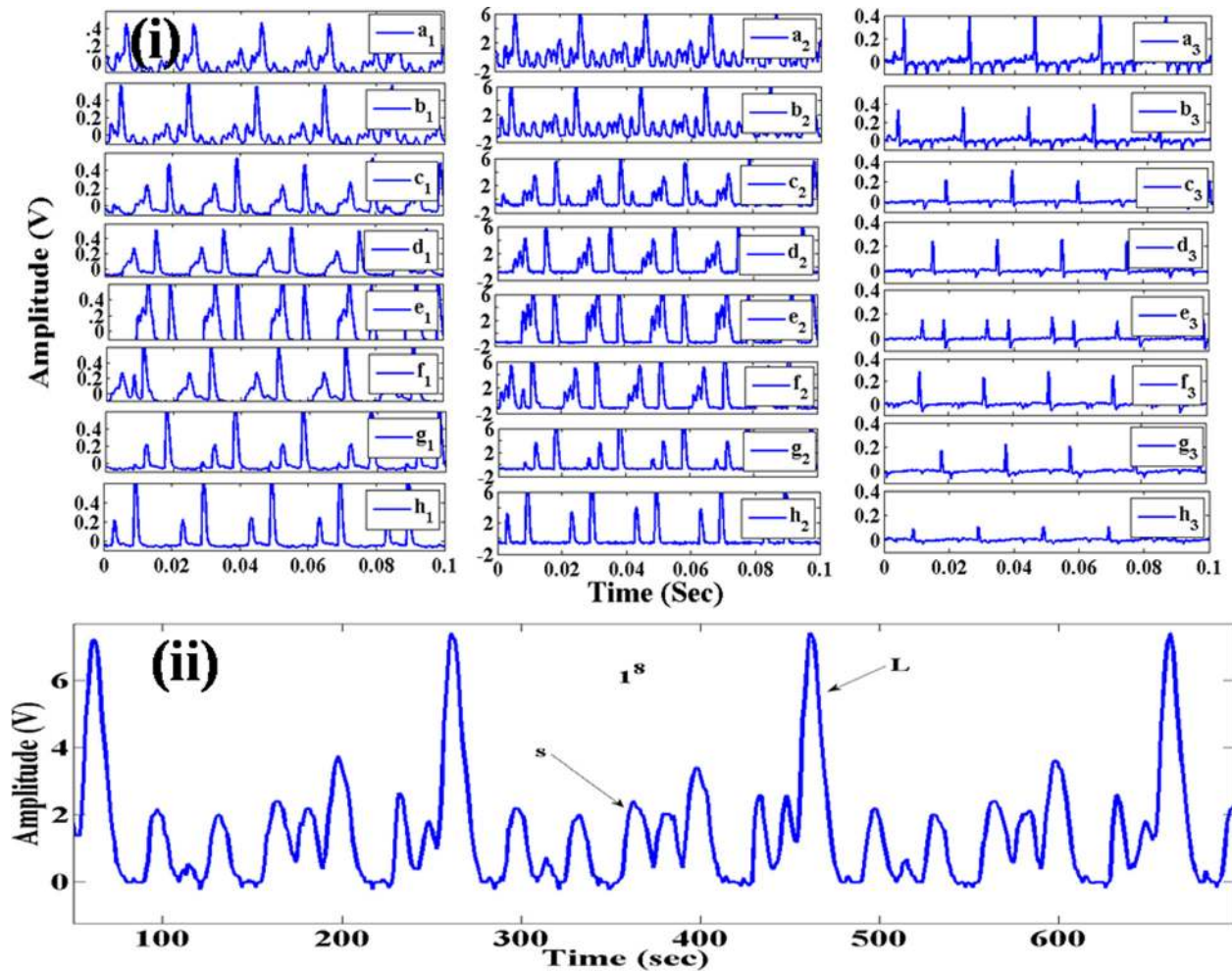


FIG. 3. (i) Represents the time series of the floating potential fluctuations obtained by the inside (a_1)–(h_1), the middle (a_2)–(h_2), and the outside Langmuir probes (a_3)–(h_3) in various magnetic fields: (a) 0 G, (b) 23 G, (c) 70 G, (d) 76 G, (e) 90 G, (f) 132 G, (g) 164 G, and (h) 198 G. (ii) Representation (Zoom) of the signal a_2 at 250 V.

oscillations changes with the probe position too. The MMOs emerge more clearly in the middle probe when compared to the other probes because the inner and outer probes are kept in the diffused plasma regime. It is also noticed that with the increase in the discharge voltage, the MMOs show more variations in the dynamics. In comparison to 240 V, at 250 V, several new states of MMOs appear as the system energy increases.

1. Spectral analysis

A power spectrum gives the initial insights about the nature of the nonlinear phenomena that evolve in real systems with the variation of the control parameters. Here, we explore how different frequency components of the floating potential fluctuations contributed to the resultant MMOs.

Fig. 4 illustrates the power spectra of the signals of the floating potential fluctuations obtained by the inner probe (a_1)–(h_1), the middle (a_2)–(h_2) probe, and the outer probe (a_3)–(h_3). The inner probe has detected the frequencies of 54 Hz, 104.9 Hz, 154.9 Hz, 204.9 Hz, 304.8 Hz, and 604.7 Hz for all magnetic fields. We find that only the amplitudes of the frequencies change with the increase in the magnetic field. The amplitudes are lying within 100 (arb. unit). We

have mainly considered the frequencies having amplitudes of more than 30 (arb. unit).

However, the middle probe signal shows a drifting amplitude from 100 to 1200 (arb. unit) for the same change in the magnetic field as the probe is kept in the bulk plasma regime. Hence, the signal strength is high in this region. Along the frequencies 54 Hz, 104.9 Hz, 154.9 Hz, 204.9 Hz, 254.9 Hz, 304.8 Hz, 354.8 Hz, and 604.7 Hz, some new frequencies such as 404.8 Hz, 454.8 Hz, 504.7 Hz, 654.7 Hz, 704.6 Hz, 754.6 Hz, and 804.6 Hz also appear in the power spectrum of the middle probe signal. These frequencies remain constant with the variation of the magnetic field.

The power spectrum of the outer probe signal shows frequencies with amplitudes less than 40 (arb. unit). With an increase in the magnetic field, the amplitudes of the frequencies declines even below 10 (arb. unit) as the LP₃ probe is kept outside the cylindrical mesh grid where only the rarefied diffused plasma exists. Hence, the signal strength is very poor in this region.

Fig. 5 shows the power spectra of the oscillations of the floating potential fluctuations obtained by the inner (a_1)–(d_1), the middle (a_2)–(d_2), and the outer Langmuir probes (a_3)–(d_3) at 240 V. The inner probe signal shows the frequencies of 54 Hz, 104.9 Hz, 154.9 Hz, 204.9 Hz, 254.9 Hz, 304.8 Hz,

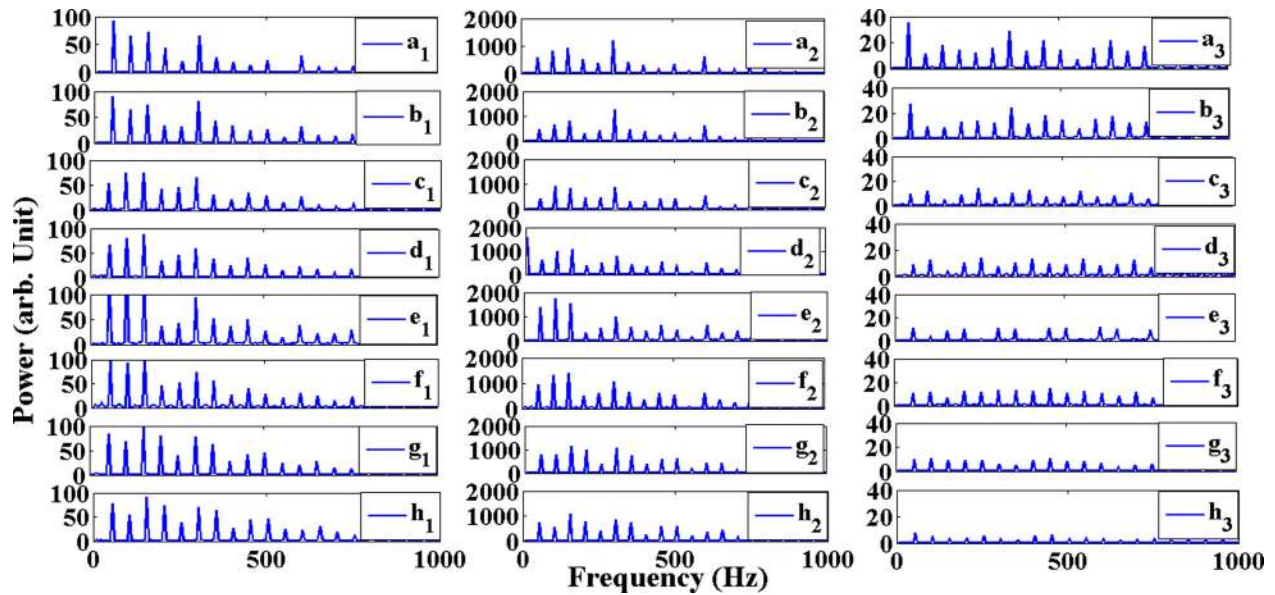


FIG. 4. FFT power spectra of the signals of the floating potential fluctuations in regimes I, II, and III at 250 V.

454.8 Hz, 504.7 Hz, and 604.7 Hz in different magnetic fields. These frequencies show variations in the amplitudes with the alteration of the magnetic field and with amplitudes of 100 (arb. unit). The frequencies detected by the power spectrum of the middle probe signal are 54 Hz, 104.9 Hz, 154.9 Hz, 204.9 Hz, 254.9 Hz, 304.8 Hz, 354.8 Hz, 404.8 Hz, 454.8 Hz, 504.7 Hz, 554.7 Hz, 604.7 Hz, 704.6 Hz, 754.6 Hz, 804.6 Hz, 854.6 Hz, and 904.5 Hz. For the middle probe signal, the amplitude of the mentioned frequencies increases to 1000 (arb. unit). The following frequencies remain invariant with respect to the magnetic field. The frequencies of the outer probe signal are equal to those observed by the LP_1 and LP_2 probes but with much less amplitude, below 20 (arb. unit). At 12 G, it even reaches 10 (arb. unit). Further, we find that the frequency variations are similar with respect to the magnetic fields in two constant discharge voltages, i.e., 240 V and

250 V, respectively (Figs. 4 and 5). Hence, the increase in the discharge voltage does not affect the instability frequencies rather it plays a crucial role in the dynamical transition of MMOs as displayed in the corresponding time series (Figs. 2 and 3).

2. Recurrence quantification analysis (RQA) of plasma oscillations

The recurrence plot (RP) analysis of nonlinear time series is a relatively new and advanced technique introduced by Takens *et al.*²⁷ Besides providing visual information, a RP also serves for the calculation of several measures of complexity associated with the different small-scale recurrent structures. A RP is based on the phase space representation of the dynamics of a dynamical system. If only a scalar

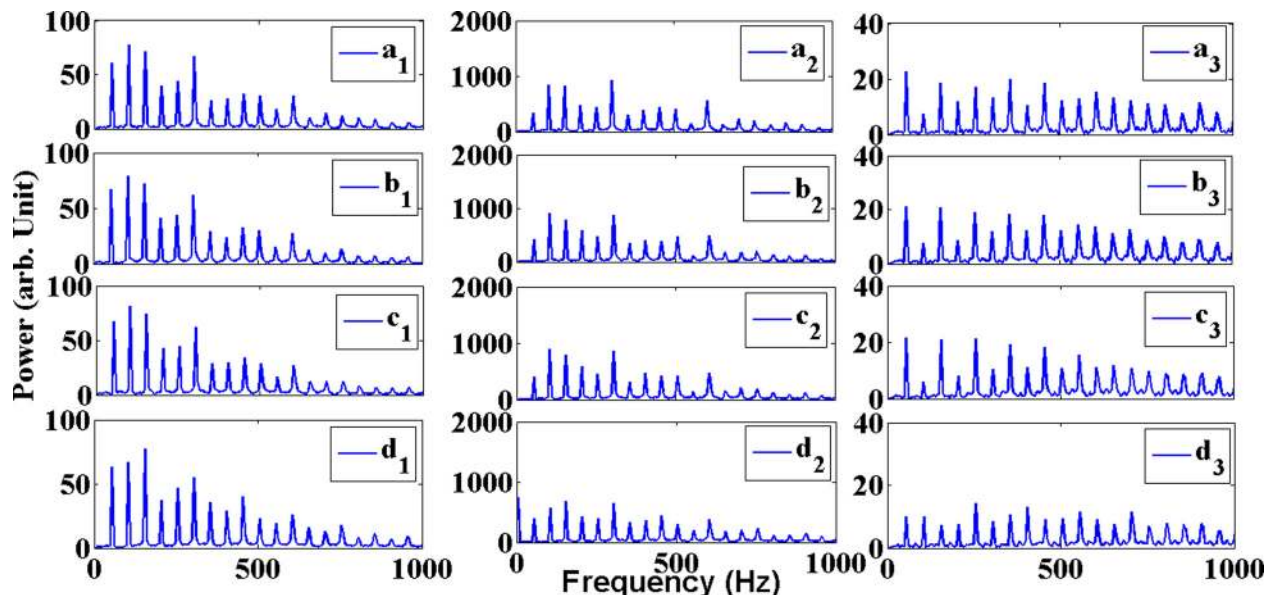


FIG. 5. FFT power spectra of the signals of the floating potential fluctuations in regimes I, II, and III at 240 V.

time series is available, the phase space can be reconstructed according to Taken's embedding theorem.²⁷ Using a time series X_i , an embedding can be made to derive the phase space vector Y_i by $Y_i = (X_i, X_{i+t}, \dots, X_{i+(d-1)t})$, where d is the embedding dimension and t is the time delay. The correct embedding parameters preserving the topological property of the original phase space are estimated by the false nearest neighbor and mutual information method.^{28,29} The original time series is now embedded into a d -dimensional reconstructed phase space. A recurrence is said to occur whenever a trajectory visits approximately the same region of the phase space. The RP is then a graphical representation of the square matrix, $R_{i,j} = H(\epsilon - \|Y_i - Y_j\|)$, where ϵ is a predetermined threshold and H is the Heaviside unit step function. Both axes of the graph represent the temporal extent to which the signal spans. Several statistical measures quantify the characteristics of the different structures appearing in a RP and are known as Recurrence Quantification Analysis (RQA). For example, the RQA measure determinism (DET) gives the ratio of the number of recurrence points that form diagonal lines in the RP to all recurrence points in the RP. For deterministic dynamics, determinism (DET) is close to unity and approaches zero when the behavior is random. Other RQA measures that are also related to diagonal lines in the RP, such as the average diagonal line length or the Shannon entropy (ENT) of the probability distribution of the diagonal line lengths, also reflect the complexity of the deterministic structures in the system.

Figs. 6(a) and 6(b) show recurrence plots of the three signals observed at 250 V when $B = 0$. We observe that the RPs of the inner and the middle probes are similar and reflect the synchronization of both signals. In both RPs, long diagonal lines can be observed, indicating large amplitude oscillations. However, some short diagonal lines are also visible in both the RPs, and these reflect the small amplitude oscillations. The RPs for regime III (outer probe) reveal some interrupted diagonal lines and single recurrence points, which are not homogeneously distributed (Figs. 6(iii-a) and 6(iii-b)). Hence, these RPs illustrate the irregular nature of the MMOs.

Next, we consider the RQA measures recurrence rate (RR), DET, and ENT for different magnetic fields (Fig. 7). RR estimates the recurrence point density in the RP. With an increase in the magnetic field, RR shows an increasing trend for all the three signals. The trend of RR for the inner and the middle probes (LP_1 and LP_2) is rather similar trend, also observed in all the other analysis. However, for the outer probe (LP_3), we observe a rise and fall of RR during the increase in the magnetic field which reflects an irregular complex nature of the dynamics.

A frequently used RQA measure to identify order to chaos transitions is DET. We find that DET increases with respect to the magnetic field, indicating that the dynamics of the plasma oscillations changes slowly towards an order state. However, an increase and a decrease are again observed for the outer probe (LP_3) signal. This might

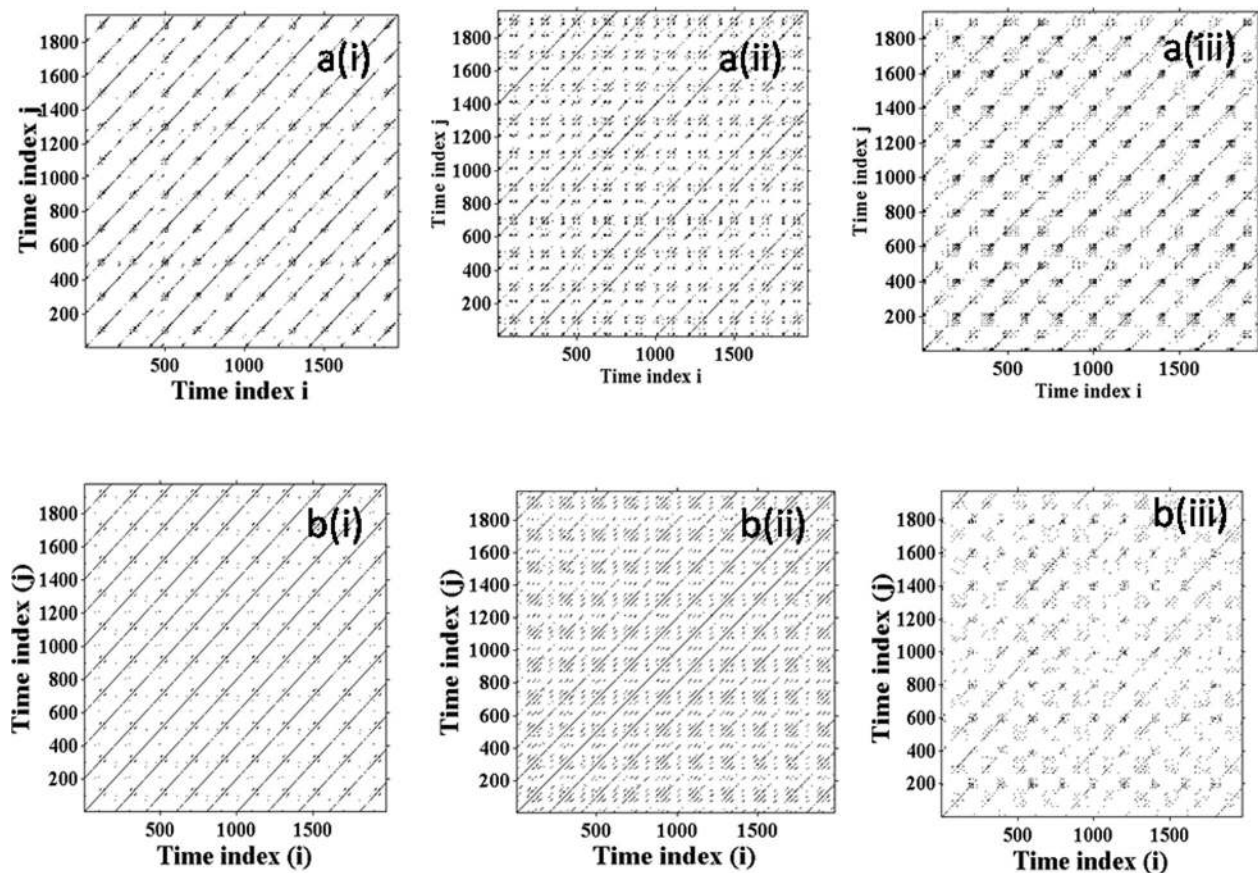


FIG. 6. (a) and (b) Recurrence plot of the floating potential fluctuations obtained in (i) regime I, (ii) regime II, and (iii) regime III at (a) 250 V and (b) 240 V with $B = 0$.

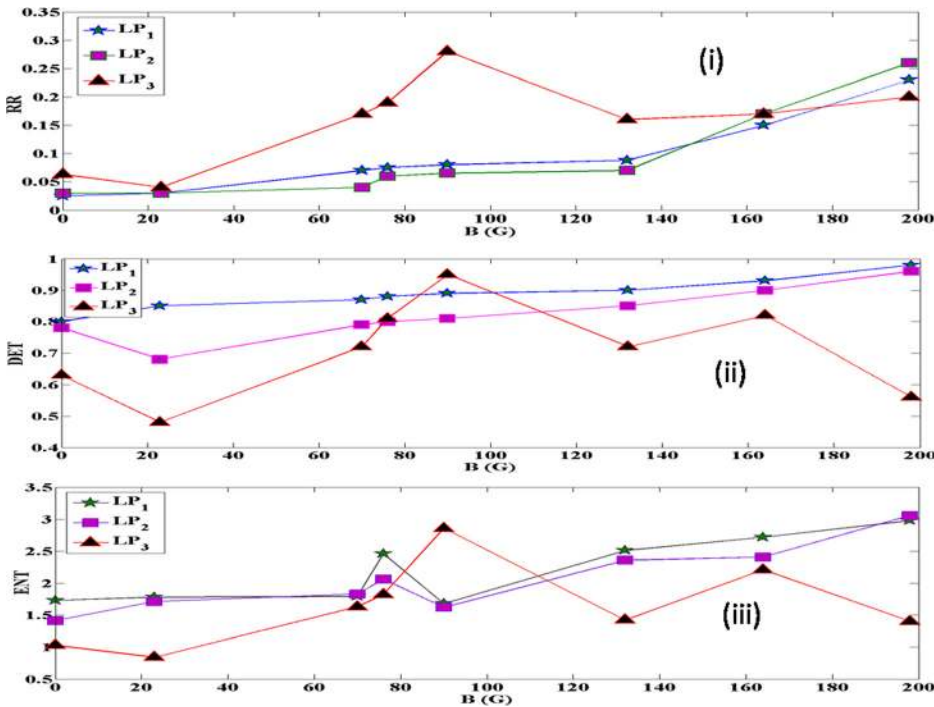


FIG. 7. Recurrence measures (i) RR, (ii) DET, and (iii) ENT of the floating potential fluctuations with respect to different magnetic fields.

indicate that the dynamics of the outer probe is more irregular and complex.

ENT measures the distribution of the diagonal line lengths. It reflects the nature of the complexity of the oscillations in the system. We also find that the ENT reflects an increasing trend for the signal of both the probes (LP₁ and LP₂). The signal of the outer probe again exhibits both an increasing and a decreasing trend. This confirms that the dynamics in the outer probe region is not following a particular order. It rather shows an irregular behaviour with the changes in the magnetic field.

All the RQA variables uncover that the signals captured by the inner and the middle probes indicate a transition from a less regular to a more regular state. Initially, small oscillations appear between two consecutive large oscillations leading to high complexity. But the enhancing magnetic field compels the dynamics of the system to move towards a more ordered state. Hence for higher magnetic fields, the RQA measures show high values as the system dynamic becomes more predictable and regular.

B. Skewness and kurtosis

The skewness quantifies the degree of asymmetry of a distribution around the mean data. There are few recent applications, where skewness and kurtosis are used to investigate the complexity of the raw data in the glow discharge plasma system.^{30,31} When a distribution looks same to both left and right from the centre point, it can be considered as a symmetric distribution. If the value of skewness is negative, the data are concentrated more to the left of the mean than to the right, and vice versa. The value of skewness of the normal distribution (Gaussian distribution) is always zero. Kurtosis estimates the peakedness or flatness of a distribution of fluctuations around the data mean. Higher and lower values of kurtosis reflect a sharper peak and flatter peak than

normal distribution, with the values concentrated around the mean of the distribution. The kurtosis of the normal distribution is 3.

Figs. 8(a) and 8(b) represent skewness and kurtosis of the inside, the middle, and the outside probe signals at 250 V. The skewness values of the inside and the middle signals increase initially from 1.82 to 2.47 and 2.09, respectively, then after 20 G, it starts to decrease slightly and drops finally at 90 G. With further increasing the magnetic field, the skewness again increases and finally reaches 3.29. The signal of the outer probe shows larger skewness values compared to the other probe signals. It increases from 3.33 to 5.28 at 76 G and then shows a sharp fall at 90 G (2.93). Skewness again increases up to 5.18 at 132 G. With the further increase in the magnetic field, it starts to fall and becomes 3.68 at 198 G.

The value of kurtosis illustrates exactly a similar trend like the skewness. Kurtosis of the two probes' signal (inside and middle) shows variation from 6.98 to 4.04 and 6.53 to 3.67 at 90 G. Kurtosis of the outer probe initially (24.22) increases with the magnetic field and reaches its maximum at 76 G (38.92). It shows a sudden dip at 90 G (17.13) and again tends to increase up to 36.32 at 132 G. For higher magnetic fields, the kurtosis again decreases and falls to a value of 24.91 at 198 G. The skewness and kurtosis of the inner and the middle probe signals illustrate almost a similar trend; only the amplitudes are different. It reflects a more flat distribution for the inner and the middle signals compared to the outer one.

We repeat this analysis of skewness and kurtosis for the floating potential fluctuations obtained at 240 V (Fig. 9). The skewness of the LP₁ and LP₂ signals are almost similar and it is consistent even in higher voltage (Fig. 9(a)). The skewness varies from 2.76 to 3.76 for the inner probe and 2.69 to 3.14 for the middle probe when the magnetic field varies

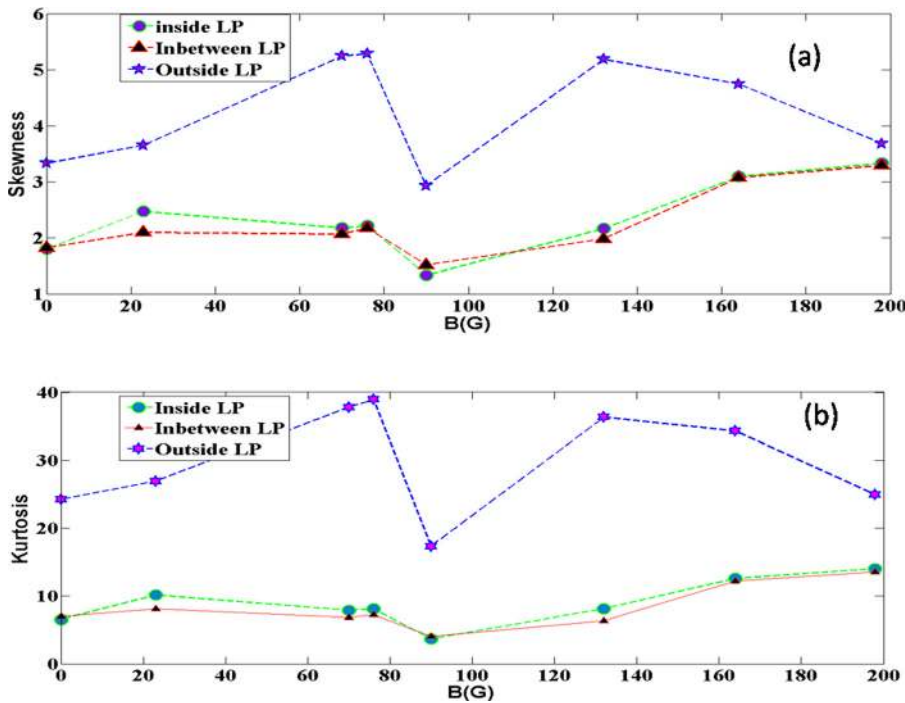


FIG. 8. (a) Skewness and (b) kurtosis of the floating potential fluctuations in different magnetic fields at 250 V.

from 0 G to 12 G. This behaviour is rather similar to the one we found for 250 V. However, the skewness of the outer probe shows huge difference when compared to the other two probes. It varies from 6.2 and has a maximum (9.22) at 12 G. With a further increase in the magnetic field, skewness starts to decrease and finally becomes 4.94 at 50 G.

The kurtosis increases from 11.12 to 18.15 for the inner probe and from 10.81 to 14.01 for the middle probe signal when the magnetic field increases from 0 to 16 G (Fig. 9(b)). The kurtosis for the inner and the middle probe signals reveals uniformity with respect to the magnetic fields, and it

unveils an almost indistinguishable trend for both the signals, which reflects that the dynamical behavior of both signals are quite close, although the corresponding signals have been obtained at different positions of the plasma system and conjectures the self similar behavior of the signals. For the case of the outer probe, a maximum is observed at 12 G (103.16), then it gradually decreases to 52.53 at 20 G, and finally reaches to 45.72 at 50 G. Hence, it reflects an initial increase in the complexity but with the further increase in the magnetic field, the complexity is suppressed as the small oscillations disappear with the increase in the magnetic field.

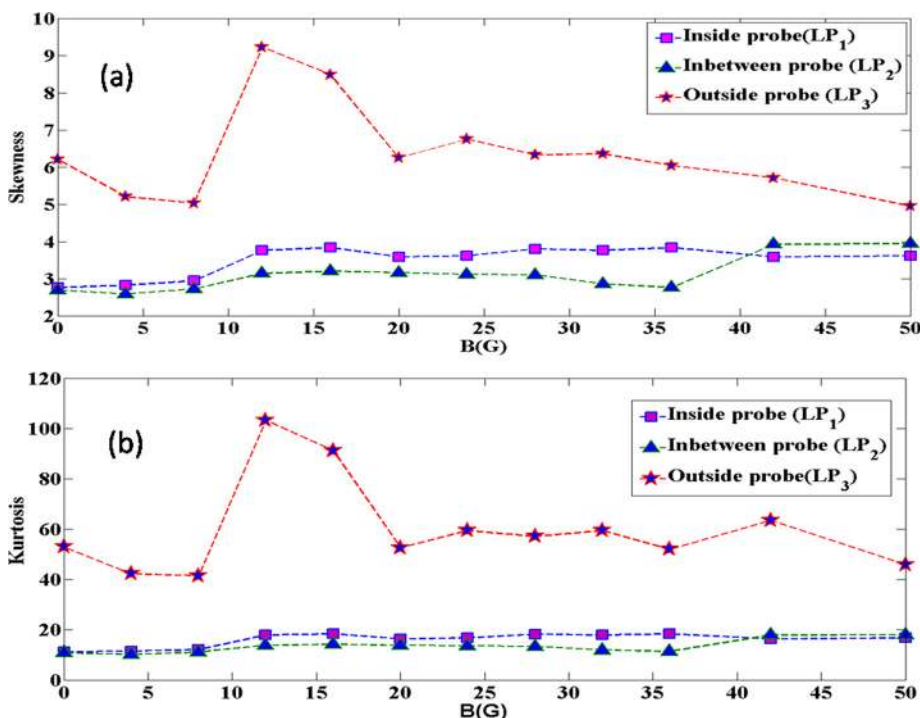


FIG. 9. (a) Skewness and (b) kurtosis of the floating potential fluctuations in different magnetic fields at 240 V.

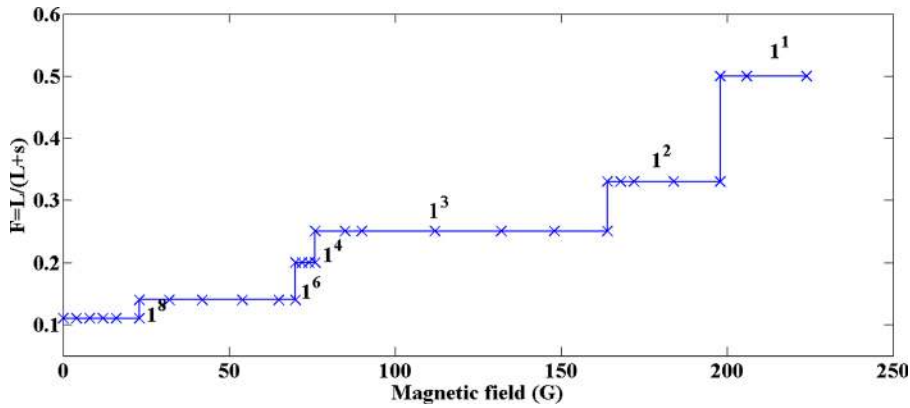


FIG. 10. Devil's staircase shows the variation in the firing number with the magnetic field at 250 V.

Figs. 8 and 9 show nearly close trends for both skewness and kurtosis. We note that this similarity in skewness and kurtosis appears only for the special cases of the MMOs.

IV. DEVIL'S STAIRCASES AND FAREY ARITHMETIC

The detailed bifurcation behavior associated with the mixed mode oscillations can be better studied by the Farey arithmetic, which delivers rational approximations of irrational numbers.^{32,33} These states can be denoted by a particular number, the Firing number (F). The ratio of the number of small amplitude oscillations to the total number of oscillations per period is characterized by the Firing number. It is defined by $F = L/(L + s)$, where L is the number of large oscillations and s is the number of small oscillations.

Fig. 10 shows the variation of F depending on the magnetic field (B) and at the constant voltage of 250 V for the middle probe signal. It clearly represents the transition from 1^8 to 1^1 states with the enhancement of the magnetic field. With the transition from 1^8 to 1^1 states, the Firing number F shows an increase from 0.16 to 0.5. However, F is not continuously increasing with B , but instead it increases stepwise with obvious jumps. This step by step evolution can be identified as devil's staircase. Among all the MMOs, the 1^3 state persists longest. Above the magnetic field at 198 G, the system shows the constant mixed mode (1^1) behaviour. Hence, the firing number is getting saturated (0.25) at 198 G.

Fig. 11 illustrates the devil staircase for the signal of the middle probe obtained at 240 V in the presence of various magnetic fields. It clearly shows the step-wise transition

from one mixed mode state (1^5) to another (1^3) by forming three steps. F increases from 0.16 to 0.26 with the change in the magnetic field. It is seen that the 1^3 state remains constant from 12 G to higher magnetic fields. Hence, the 1^3 state persists for long time duration compared to the other two steps. A similar behaviour was observed at 250 V, but we also observed more mixed mode oscillations than at 240 V.

V. CONCLUSION

In summary, it has been shown that the mixed mode oscillations are excited due to the magnetized inverted fireball developed in the low temperature glow discharge plasma system. In this study, mixed mode oscillations are characterized inside and outside the constricted spherical anode and cylindrical cathode in the presence of the magnetic field. This work highlights the rich dynamics of the MMO with the variation of the magnetic field in different discharge voltages. The making and breaking mechanism of the inverted fireball (anode glow) is influenced by the magnetic field, which controls the dynamics of the floating potential fluctuations and suppresses the small amplitude oscillations. The magnetic field introduces the anisotropy in the particle dynamics. The signal obtained at different positions of the plasma system helps to understand the spatiotemporal dynamics of the plasma oscillations. Synchronization of the floating potential fluctuations is clearly observed in the inner and the middle probe signals. The outer probe is far from the spherical ball (inverted fireball); hence, the signal of the outer probe is irregular and not similar to the other two probes.

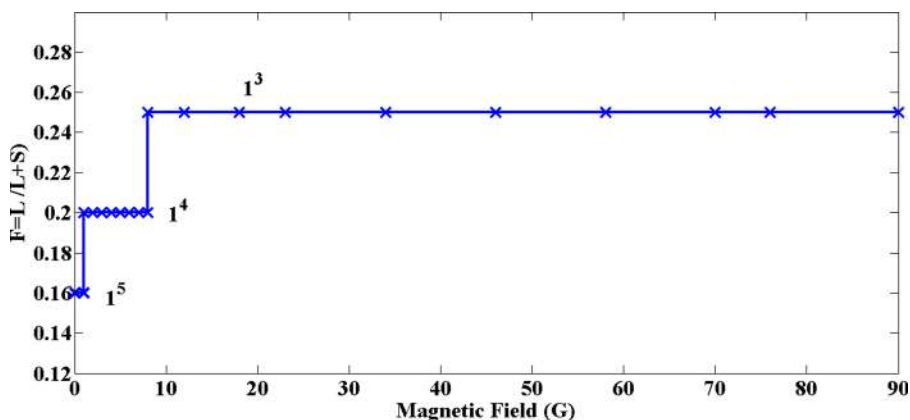


FIG. 11. Devil's staircase represents the changes in the firing number with the magnetic field at 240 V.

The RP reflects the appearance of MMOs in the dynamics of floating potential fluctuations as the small diagonals appear between the large non interrupted diagonal lines. The considered RQA measures tend to increase while the magnetic field is increased. This finding suggests that the oscillations become ordered as the small oscillations of MMOs are suppressed. The incomplete devil staircase has been observed at both 240 V and 250 V. It reflects clearly the MMO features, which are supportive of other analysis, such as power spectrum and recurrence plot.

ACKNOWLEDGMENTS

The authors are thankful to BRNS-DAE, Government of India for the financial support under the project grant (Reference No. 2013/34/29/BRNS). The authors would like to thank the referees for their fruitful suggestions that helped to improve the quality of the paper.

- ¹G. Popa and R. Schrittwieser, *Phys. Plasmas* **1**, 32 (1994).
- ²N. Ohno, K. Komori, M. Tanaka, and Y. Kawai, *Phys. Fluids B* **3**, 228 (1991).
- ³R. L. Stenzel, *Phys. Fluids B* **1**, 2273 (1989).
- ⁴A. Sarma, H. Bailung, and J. Chutia, *Phys. Plasmas* **4**, 61 (1996).
- ⁵J. Chutia, S. Sato, H. Kubo, and Y. Nakamura, *J. Plasma Phys.* **46**, 463 (1991).
- ⁶B. Singha, A. Sarma, and J. Chutia, *Phys. Plasmas* **9**, 683 (2002).
- ⁷Y. P. Bliokh, J. Feltsteiner, and Y. Z. Slutsker, *J. Appl. Phys.* **111**, 013302 (2012).
- ⁸P. J. Barrett and R. G. Greaves, *Phys. Fluids B* **1**, 1776 (1989).
- ⁹H. Klostermann, A. Rohde, and A. Piel, *Phys. Plasmas* **4**, 2406 (1997).
- ¹⁰T. Gyergyek, M. Cercek, R. Schrittwieser, and C. Ionita, *Controlled Plasma Phys.* **42**, 508 (2002).
- ¹¹D. G. Dimitru, M. Aflori, L. M. Ivan, C. Ionita, and R. W. Schrittwieser, *Plasma Phys. Controlled Fusion* **49**, 237 (2007).
- ¹²R. L. Stenzel, C. Ionita, and R. Schrittwieser, *Plasma Sources Sci. Technol.* **49**(17), 035006 (2008).
- ¹³C. Ionita, D. Dimitriu, and R. Schrittwieser, *Int. J. Mass Spectrom.* **233**, 343 (2004).
- ¹⁴R. L. Stenzel, C. Ionita, and R. Schrittwieser, *J. Appl. Phys.* **109**, 113305 (2011).
- ¹⁵R. L. Stenzel, J. Gruenwald, B. Fonda, C. Ionita, and R. Schrittwieser, *Phys. Plasmas* **18**, 012104 (2011).
- ¹⁶R. L. Stenzel, J. Gruenwald, B. Fonda, C. Ionita, and R. Schrittwieser, *Phys. Plasmas* **18**, 012105 (2011).
- ¹⁷J. Gruenwald, *Phys. Plasmas* **21**, 082109 (2014).
- ¹⁸V. Mitra, B. Sarma, A. Sarma, M. S. Janaki, and A. N. Sekar Iyengar, *Phys. Plasmas* **23**, 032304 (2016).
- ¹⁹J. Chopin-Duman, *C. R. Acad. Sci. (Paris) C* **287**, 553 (1978).
- ²⁰T. Braun, J. A. Lisboa, and J. A. C. Gallas, *Phys. Rev. Lett.* **68**, 2770 (1992).
- ²¹T. Hayashi, *Phys. Rev. Lett.* **84**, 3334 (2000).
- ²²M. Mikikian, M. Cavvaroe, L. Couedel, Y. Tessier, and L. Boufendi, *Phys. Rev. Lett.* **100**, 225005 (2008).
- ²³S. Chakraborty and S. K. Dana, *Chaos* **20**, 023107 (2010).
- ²⁴S. Ghosh, P. K. Shaw, D. Saha, M. S. Janaki, and A. N. Sekar Iyengar, *Phys. Plasmas* **22**, 052304 (2015).
- ²⁵P. K. Shaw, A. N. Sekar Iyengar, and Md. Nurujjaman, *Phys. Plasmas* **22**, 122301 (2015).
- ²⁶J.-P. Eckmann, S. O. Kamphorst, and D. Ruelle, *Europhys. Lett.* **4**, 973 (1987).
- ²⁷F. Takens, *Lecture Notes in Mathematics* (Springer, 1981), Vol. 898, p. 366.
- ²⁸N. Marwan, M. C. Romano, M. Thiel, and J. Kurths, *Phys. Rep.* **438**, 237 (2007).
- ²⁹S. Schinkel, N. Marwan, O. Dimigen, and J. Kurths, *Phys. Lett. A* **373**, 2245 (2009).
- ³⁰V. Mitra, A. Sarma, M. S. Janaki, A. N. Sekar Iyengar, B. Sarma, N. Marwan, J. Kurths, P. K. Shaw, D. Saha, and S. Ghosh, *Chaos, Solitons Fractals* **69**, 285 (2014).
- ³¹A. M. Wharton, A. N. Sekar Iyengar, and M. S. Janaki, *Phys. Plasmas* **20**, 022301 (2013).
- ³²J. Maselko and H. L. Swinney, *J. Chem. Phys.* **85**, 6430 (1986).
- ³³V. Petrov and K. Shower, *J. Chem. Phys.* **97**, 6191 (1992).